



HAL
open science

Effect of the presence of solid particles, on the vanadyl sulfate (VOSO₄) oxidation current

Yendoube Charles Sano Moyeme, Ranine El Hage, Ali Hassan, Fabien Chauvet, Laurent Cassayre, Béatrice Biscans, Delphine Quaranta, Théo Tzedakis

► To cite this version:

Yendoube Charles Sano Moyeme, Ranine El Hage, Ali Hassan, Fabien Chauvet, Laurent Cassayre, et al.. Effect of the presence of solid particles, on the vanadyl sulfate (VOSO₄) oxidation current. *Electrochimica Acta*, 2021, 373, pp.137909. 10.1016/j.electacta.2021.137909 . hal-03194299

HAL Id: hal-03194299

<https://hal.science/hal-03194299>

Submitted on 9 Apr 2021

HAL is a multi-disciplinary open access archive for the deposit and dissemination of scientific research documents, whether they are published or not. The documents may come from teaching and research institutions in France or abroad, or from public or private research centers.

L'archive ouverte pluridisciplinaire **HAL**, est destinée au dépôt et à la diffusion de documents scientifiques de niveau recherche, publiés ou non, émanant des établissements d'enseignement et de recherche français ou étrangers, des laboratoires publics ou privés.











Open Archive Toulouse Archive Ouverte (OATAO)

OATAO is an open access repository that collects the work of Toulouse researchers and makes it freely available over the web where possible

This is an author's version published in: <http://oatao.univ-toulouse.fr/27640>

Official URL: <https://doi.org/10.1016/j.electacta.2021.137909>

To cite this version:

Sano Moyeme, Yendoube Charles  and El Hage, Ranine  and Hassan, Ali 
and Chauvet, Fabien  and Cassayre, Laurent  and Biscans, Béatrice  and
Quaranta, Delphine  and Tzedakis, Théo  *Effect of the presence of solid
particles, on the vanadyl sulfate (VOSO₄) oxidation current.* (2021)
Electrochimica Acta, 373. 137909. ISSN 0013-4686

Any correspondence concerning this service should be sent
to the repository administrator: tech-oatao@listes-diff.inp-toulouse.fr

Effect of the presence of solid particles, on the vanadyl sulfate (VOSO_4) oxidation current

C.Y. Sano Moyeme, R. El Hage, A. Hassan, F. Chauvet, L. Cassayre, B. Biscans, D. Quaranta, T. Tzedakis*

Laboratoire de Génie Chimique, UMR CNRS 5503, Université de Toulouse, CNRS, INP, UPS, Toulouse, France

ARTICLE INFO

Keywords:

Vanadium redox batteries
 VO^{2+} oxidation current
Liquid-solid suspension
Vanadium sulfate solid particles
Ketjen black nanoparticles

ABSTRACT

This study considers the effect of mechanical stirring of $\text{V}^{(IV)}$ solutions and of the presence of solid suspensions on the $\text{VO}_{(aq)}^{2+}$ oxidation current measured on a graphite electrode, with the objective of a better understanding of the electrochemical reactions taking place in a vanadium redox flow battery (VRFB). Our research question was to determine whether the presence of different kind of solid particles (inert glass spheres, VOSO_4 powder and nanometric ketjen black (KB)) could be beneficial to the electrochemical performances of the VRFB. The experimental method consisted in measuring the anodic limiting current of a $\text{VO}\text{SO}_4\text{-H}_2\text{SO}_4\text{-H}_2\text{O}$ solution on a rotating graphite cylinder, by linear sweep voltammetry.

In the absence of solid particles, we show that the mass transfer coefficient dependence against the angular velocity of both the electrode and an additional stirrer obey to a power law ($k = f(\omega^\gamma)$) with an exponent γ found to be lower than the theoretical value. The beneficial effect on the mass transfer of VO^{2+} at the interface observed with low fraction of inert glass particles dramatically disappears as the spheres fraction increases. This is attributed to the decrease of the available free volume for the diffusion. When the solid consists of VOSO_4 particles, the anodic current decreases as the mass fraction of the solid increases, which demonstrates the absence of any significant beneficial effect of the dissolution of the VOSO_4 grains in the diffusion layer. Conversely, an important increase ($\sim 40\%$) of the oxidation current is observed when KB particles were introduced at low fractions (0.15%) in the bulk, thanks to the electronic percolation created by the KB. However, this beneficial effect disappears for higher mass fraction of both vanadium or KB solid particles, because of the destruction of the aggregates enabling the electron to be driven into the bulk.

1. Introduction

In recent years, sources of renewable energies have been involved to supply 'green' energy for human uses. However, their intermittency is considered to be a major disadvantage and adequate technologies should be developed to store this energy and restore it according to demand. Amongst the various techniques potentially used to store electrical energy, the electrochemical storage has a number of advantages [1]. Technologies such as redox flow batteries (RFB) gained new interest in recent years. Their particularity is that the reactive species are stored outside the reactor, in storage tanks, thus enabling to increase the amount of energy stored, by increasing both the capacity of the storage tanks and also the concentration of the active species. The RFB enables an

ideal power / energy decoupling, thus facilitating the design of industrial units for energy production and transformation [2].

The all vanadium redox flow batteries (VRFB) involve vanadium electroactive species in four different oxidation states; This characteristic enables to avoid irreversible cross-contamination that constitutes a major drawback for other RFBs, such as Fe/Cr systems [3–5]. However, the main disadvantage of this battery is related to the low quantity of electroactive material stored per unit of volume; Thus the commercial VRFB delivers around 45 Wh/L [6,7], which is more than three folds lower than the energy claimed for solid Li-ion battery ~ 150 Wh/kg [8] (without flow). This is mainly due to the limited solubility of vanadium salts (~ 2 M), strongly depending on the vanadium valence, the temperature and the sulfuric acid concentration usually used as supporting electrolyte for the first generation of VRFB [9,10]. Various methods have been proposed to overcome this problem: The use of a mixed acid supporting electrolyte $\text{HCl} - \text{H}_2\text{SO}_4$ [11] or $\text{CH}_3\text{SO}_3\text{H} - \text{H}_2\text{SO}_4$ [12], and the addi-

* Corresponding author.

E-mail address: tzedakis@chimie.ups-tlse.fr (T. Tzedakis).

Nomenclature

a, a', a'':	constants
b, b' and b'':	constants
AE:	auxiliary (or counter) electrode
F:	faraday constant (96,500 C.mol ⁻¹)
E:	potential (V). Without any specific indication, all the potentials were expressed versus the SCE
EIS:	electrochemical impedance spectroscopy
CSS:	cross shaped stirrer
C:	molar concentration (mol.L ⁻¹ , or M)
D and D _{eff} :	'diffusion' and 'effective diffusion' coefficients (m ² .s ⁻¹)
d _{glasses} :	mean diameter of the glass spheres (m)
d _e :	characteristic length (m)
I, I _{lim} :	current and limiting current (A)
k:	mass transfer coefficient (m.s ⁻¹) = a' + b' × ω ^γ ⇒ I _{lim} = a'' × S + b''S × ω ^γ ,
N _{glasses} :	number of glass spheres per cm of distance, in a direction between the wall of the cell and the axis of the RCE
n:	electron number
r:	potential scan rate (V.s ⁻¹)
Re:	reynolds number = v ρ d _e / μ
RFB:	redox Flow Batteries
RCE:	rotating Cylinder Electrode (here used as the WE graphite made).
S:	surface (m ²)
Sc:	schmidt number = ν / D
SCE:	saturated calomel electrode (here used as reference electrode)
Sh:	sherwood number = k d _e / D = a + b × Re ^γ × Sc ^κ = the Leveque correlation
T:	temperature (°C)
VRFB:	vanadium redox flow batteries
WE:	working electrode
γ and κ	constants dependant of the system (for simple geometries such as the disc: γ=1/2 and κ=1/3)
ε:	volume fraction available for diffusion
λ and λ':	constants in the equation I _{lim} as a function of ω
μ and ν:	dynamic and kinematic viscosities respectively (Pa.s and m ² .s ⁻¹ , respectively)
ρ:	specific gravity (kg.m ⁻³)
s:	solubility (mol.L ⁻¹ , or M)
τ:	tortuosity (real trajectory/normalized trajectory)
v:	velocity (m.s ⁻¹)
Φ:	volumetric fraction of the solid in the suspension
ω:	angular velocity (RPM or rad/s)

tion of stabilizing agents in order to prevent or reduce the precipitation of vanadium species [13].

Nevertheless, the stability of vanadium solutions is still compromised by the precipitation of one of the four oxidation states at least, as they do not have the same behaviour as a function of the operating conditions [14]. Typically V^(V) exhibits the lowest solubility (s) and can precipitate as a function of the state of charge of the battery (the solubility s increases when the temperature decreases and the sulfuric acid concentration increases),

while V^(II), V^(III) and V^(IV) have an opposite behaviour (the solubility s increases when the temperature increases and the sulfuric acid concentration decreases) [9]. The precipitation of any of the redox vanadium specie can induce negative effects on the overall performance of the battery: Capacity losses, increasing resistance, cluster formation, membrane degradation due to particles collisions, etc. [9]. Moreover, the granulometry of the generated solids strongly depends on the operating conditions.

However, the impact of the presence of these solid particles on the electrochemical behaviour of the electroactive species has not been studied extensively and this constitutes the general purpose of the present study: To understand the effect of an eventual precipitation of the vanadium salts on the battery current. More precisely, our research question is to determine whether the presence of solid particles could be beneficial to the electrochemical performances of the VRFB, by contributing to (i) increase the mass transfer and (ii) compensate the depletion of the concentration in the diffusion layer. Moreover, the present study aims at examining the effect of solid particles on the electrode current in the case where a specific 'liquid-solid' suspension involves an electroactive material.

To achieve these objectives, it was chosen to quantify the effect of various solid particles (inert glass spheres, solid vanadium grains and nanometric ketjen black (KB)) by measuring by voltammetry the steady state oxidation current of V^(IV) on a rotating graphite cylinder electrode (RCE) inserted into a classical three electrodes cell. When required the cell was equipped with a cross-shaped stirrer (referred as CSS) to ensure a homogeneous distribution of the particles. The V^(IV)/V^(V) redox couple was selected because the V^(IV) oxidation current can be measured using simpler operating conditions with comparison to V^(II)/V^(III), which requires an inert atmosphere.

The studies were carried out in order to examine the effect of each type of particles on different physicochemical phenomenon:

- The effect of the collisions generated by the glass spheres on the mass transport of the dissolved VO²⁺ at the interface;
- The ability of solid VOSO₄ particles to supply VO²⁺, by dissolution, at the depleted interface and thus to contribute to enhance the current (in addition to the effect of collisions);
- The enhancement of the current by electronic percolation generated by the KB nanoparticles; indeed, in this case it is suspected that the nanoparticles create an electric frame enabling an extension of the electrode in solution and thereby the increase of the electrochemical active surface area (leading to an increase of the current).

2. Material and methods

2.1. Vanadium (IV)

The vanadium (IV) solution was prepared in 3 M sulfuric acid [14], with the following chemicals:

- Vanadium (IV) sulfate oxide pentahydrate VOSO₄•5H₂O from VWR Chemicals (technical, 97%) and from CHEMOS (technical, 97%);
- NormaPur H₂SO₄ supplied from Sigma Aldrich;
- Ultrapure water

The solution saturated by V^(IV) contains the salt at its reported solubility i.e. 1.5 M [10]. The operating temperature was chosen at 10 °C to avoid any precipitation of the product (VO₂)₂SO₄ at the electrode. Indeed, its solubility increases when the temperature decreases [15].

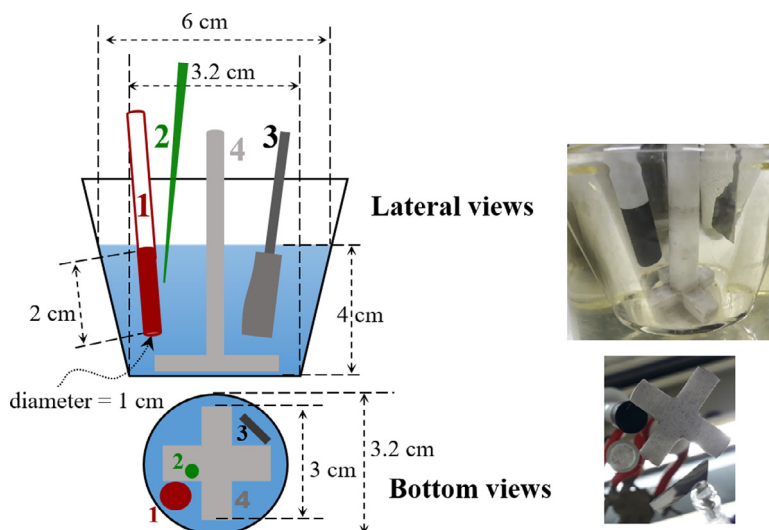


Fig. 1. Left: Sketch of the experimental setup as seen directly through the cell (lateral view) and from the bottom of the cell (bottom view); 1 = working electrode, 2 = Luggin capillary containing the reference electrode (SCE), 3 = counter electrode, 4 = additional cross shaped stirrer. **Right:** Photos of the setup.

2.2. Solid particles

Several solid-liquid suspensions, at various mass fractions were prepared by mixing solid particles with the vanadium (IV) saturated solution.

The following particles were used:

- Glass spheres with a specific gravity of $\sim 1.1 \text{ g/cm}^3$ and a granulometry in the range of $9 < d_{\text{glass spheres in } \mu\text{m}} < 13$ (average diameter = $11 \mu\text{m}$).
- Solid particles of $\text{VOSO}_4 \cdot 5\text{H}_2\text{O}$ with a specific gravity of 2.5 g/cm^3 and a granulometry in the range of $\sim 3 < \text{mean particle diameter in } \mu\text{m} < \sim 600$. Same provider as above.
- Ketjen black nanoparticles (KB, EC-600JD, n° 41,611,374, AkzoNobel) is introduced into a solution of $\text{V}^{(\text{IV})}$ containing or not $\text{VOSO}_4 \cdot 5\text{H}_2\text{O}$ solid particles in H_2SO_4 at 3 M. The mixture was stirred overnight, until obtaining a totally wet powder (validated by a sedimentation of the KB in the absence of stirring). Under stirring the KB powder is uniformly distributed into the solid and no flocs were observed.

2.3. Experimental setup

The potentiostat used is a VOLTALAB PGZ 100/ potentiostat/galvanostat *VoltaMaster* controlled by the *voltmaster 4* software. The experiments were carried out in a conventional three electrode cell from Metrohm (Fig. 1) having 100 cm^3 of capacity and the following electrodes were used:

- Working electrode: Graphite cylinder screwed on the body of a classical rotating electrode assembly to form a RCE. The used rotation frequencies are in the range of 300–1500 RPM. The geometric surface area of the working electrode is 7.07 cm^2 (sum of both the lateral area of the cylinder and the surface of the disc forming its base).
- A saturated calomel electrode (SCE) was used as reference electrode for all the experiments; It is immersed into a Luggin capillary tube containing the supporting electrolyte (3 M H_2SO_4). Because of the particular shape of the working electrode, we chose to locate the extremity of the Luggin capillary at $\sim 1 \text{ mm}$ of the middle of the lateral area of the graphite cylinder for all experiments (see Fig. 1).
- A platinum plate with 2.25 cm^2 / face of geometrical surface area was used as auxiliary electrode and located in front of

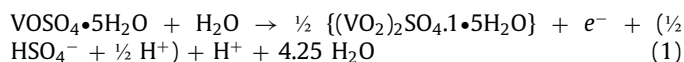
the RCE. The used potentiostat is powerful enough, enabling to manage the system without any limitation caused by the relatively small surface of the counter electrode compared to that of the working electrode.

Special care is taken to keep always the same positions of the electrodes for all the experiments. Besides, ohmic drop compensation was performed on the basis of the value of the resistance of the solution between WE and RE; This resistance was measured by electrochemical impedance at the OCP.

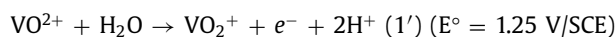
In order to maintain a uniform (fluidized) suspension, possibly containing high fractions of vanadium sulphate solid particles, it is necessary to have an efficient stirring system. The rotation of the RCE is insufficient to ensure a perfect mixing of the suspension that is why an additional PTFE-made stirrer (CSS cross-shaped) was manufactured and used (Fig. 1); Its diameter is 3 cm, and the blades are 4 mm thick. It is also fixed on a rotating electrode body, in order to control the stirring rate in the same way as the RCE.

3. Results and discussion

The 'global' half electronic reaction (1) assumed to occur at the working electrode is:



In a simplified form, assuming the dissociation of the $\text{VOSO}_4 \cdot 5\text{H}_2\text{O}$ to VO^{2+} (in fact to the complex $[\text{VO}(\text{H}_2\text{O})_5]^{2+}$ [10, 16]), the reaction (1) can be written as following:



Note that this reaction releases 5 molecules of water from the dissociation of the $\text{VOSO}_4 \cdot 5\text{H}_2\text{O}$ and captures 1.5 for the $(\text{VO}_2)_2\text{SO}_4 \cdot 1 \cdot 5\text{H}_2\text{O}$ (results in press). The reduction of $\text{VOSO}_4 \cdot 5\text{H}_2\text{O}$ occurs at the counter electrode.

This section is structured in two parts: The first one (3.1) concerns the study of the effect on the vanadium oxidation current, of the stirring of vanadium solutions by both the RCE and the CSS; A similar study was carried out in the second part (3.2) in the presence of three different solid particles (each one devoted to the study of the effect of one parameter): (i) inert glass spheres, (ii)

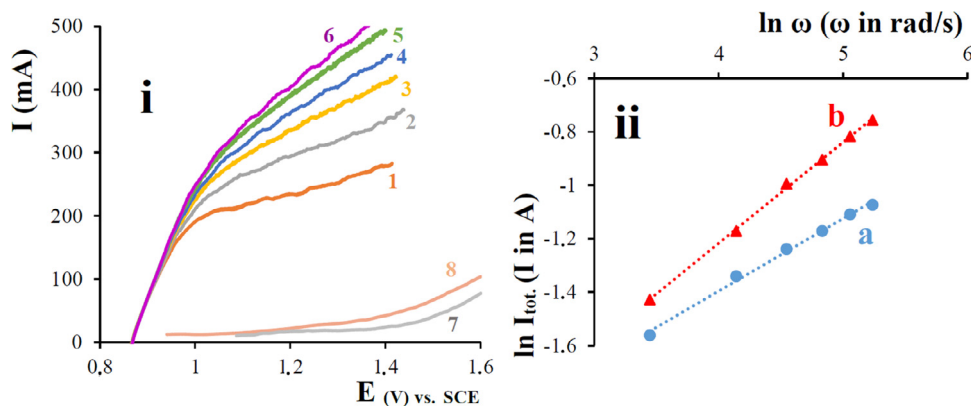


Fig. 2. i: Effect of the stirring rate of the working electrode on the shape of the current-potential curves obtained at the quasi-steady state for the oxidation of a solution of $V^{(IV)}$ to $V^{(V)}$. $\omega = 300, 600, 900, 1200, 1500, 1800$ RPM for the curves $I = f(E)$ 1 to 6, respectively. Curves 7 and 8: residual current at respectively 1200 and 1800 RPM. Primary data: $[V^{(IV)}] = 1.5 \text{ mol.L}^{-1}$ in $[H_2SO_4] = 3 \text{ mol.L}^{-1}$; $S_{WE} = 7.07 \text{ cm}^2$; $r = 10 \text{ mV.s}^{-1}$; $T = 10 \text{ }^\circ\text{C}$; WE = rotating cylindrical electrode graphite made (RCE) (diameter 1 cm, height 2 cm); AE = Pt. Ohmic drop corrected (EIS).

ii: Evolution of $\ln(I)$ as a function of $\ln(\omega)$, where ω is the angular velocity of the electrode; the currents were extracted from graph (i) without subtraction of the residual current. **a:** $\ln I$ at 1.1 V, in A = $f(\ln \omega)$; **b:** $\ln I$ at 1.3V, in A = $f(\ln \omega)$.

solid particles of the $VOSO_4 \cdot 5H_2O$ and (iii) ketjen black nanoparticles.

3.1. Characterization of the $V(IV)$ oxidation current without solid

3.1.1. Effect of the stirring rate of the working electrode on the current – potential curves for the $V^{(IV)}$ oxidation without particles

Since the experimental setup contains two elements (RCE and CSS) that are not usually used for electrochemical studies, it is important to understand the effect of the coupled stirring on the current of the vanadium oxidation. First, the effect of the stirring rate of the RCE was studied without rotation of CSS from the current-potential curves of a saturated vanadium solution at $10 \text{ }^\circ\text{C}$.

In Fig. 2i, it is shown that increasing the angular velocity in the range from 300 to 1800 RPM causes the current to increase more than twice. For angular rates lower than 600 RPM, the $I = f(E)$ curve exhibits a classical form, with a plateau ($1.08 < E_{(V)} < 1.4$) corresponding to a mass transfer limitation. Increasing the angular velocity of the electrode causes the curves to be deformed, the slope of the plateau is not constant. The latter increases with the rotation frequency (see also Fig. 2ii), thus suggesting that the (average) mass transfer coefficient depends not only on the stirring intensity but also on the applied potential or the flowing current. This seems strange, because the oxidation of the $V^{(IV)}$ to $V^{(V)}$ curve exhibits a plateau with a constant limiting current [17,18].

One plausible explanation could be the modification of the interfacial concentration of H^+ , because according to the reaction (1 or 1'), two H^+ were generated by oxidized vanadium. The increase of the acid concentration causes the enhancement of the residual current which overlaps with the vanadium current and leads to the curve deformation.

The Fig. 2ii clearly shows a linear evolution of the natural logarithm of the current against the natural logarithm of the angular velocity ω . The magnitude of the current was measured at the beginning of the plateau i.e. 1.1 V (see curve 1, Fig. 2) and at the beginning of the oxidation of the solvent i.e. 1.3 V (see curve 7 and 8, Fig. 2). As indicated above, the slopes of the straight lines increase when the potential where the current was read increases.

$$\mathbf{a:} \ln I_{\text{at } 1.1 \text{ V, in A}} = -2.48 + 0.27 \times \ln \omega_{\text{rad/s}} \quad R^2 = 0.995 \quad (2)$$

$$\mathbf{b:} \ln I_{\text{at } 1.3 \text{ V, in A}} = -2.73 + 0.38 \times \ln \omega_{\text{rad/s}} \quad R^2 = 0.999 \quad (3)$$

It is important to mention that:

- The current picked at two different potentials of the $I = f(E)$ curves can be considered as a limiting current $I_{lim} = n F S k C_{V^{(IV)}}$, where k is mass transfer coefficient, expressed as a power law of the angular velocity of the stirrer:

$$k = a + b \times \omega^\gamma \Rightarrow I_{lim} = a \times S + b S \times \omega^\gamma \quad (4)$$

(See appendix)

the magnitudes of these slopes (0.27 and 0.38) are lower than the slope predicted by the Levich correlation ($I_{lim} = f(\omega^{0.5})$) for a rotating disc electrode in very well defined conditions [19–21].

- The working electrode is a rotating cylinder having two electroactive areas: The bottom section which is a disc and its peripheral/cylindrical area. The measured limiting current is a contribution of both faces of the electrode, and the relative contribution of each part needs to be determined.

We will try to get a better understanding of the electrodes' behaviour in the following sections.

3.1.2. Respective contributions of the disc and the cylinder faces of the working electrode on the $V^{(IV)}$ oxidation current

Current potential curves were plotted for various conditions (Fig. 3i) in order to try to examine independently the effects of both the disk and the cylinder surfaces of the working electrode, on the mass transfer under stirring conditions. The solution used is the $V^{(IV)}$ at saturation (1.5 M). To that end the RCE was prepared in two ways:

- The disk was insulated with a thin adhesive scotch tape and the curves $I = f(E)$ were plotted for the external cylindrical surface, see Fig. 3i curves 1 to 6C.
- The external cylindrical surface was isolated with the same thin adhesive tape, trying to avoid any modification of the geometry of the cylinder (i.e. no roughness, the whole tape surface is completely smooth); Then the $I = f(E)$ curves were plotted on the disk active face and presented in Fig. 3i, curves $I = f(E)$ 1 to 6D.

The first observation is that the magnitude of the current measured with the cylinder alone (curves 1 to 6C) is about 5 to 6 times higher than the current measured with the disc alone (curves 1 to 6D). Besides, the surface ratio (S_c / S_d) between the cylinder and the disc is equal to ~ 8 . Taking into account that the limiting current is proportional to the surface area and to the mass transfer

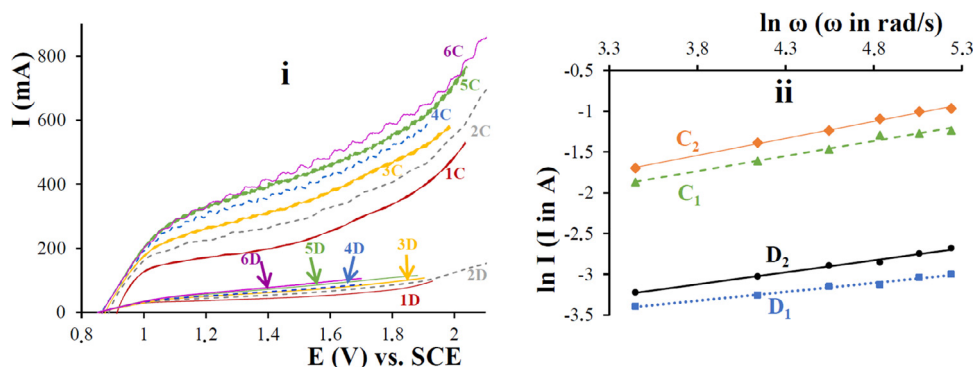


Fig. 3. i: Effect of the stirring rate of the working electrode (RCE) on the shape of the current-potential curves obtained at the quasi-steady state for the oxidation of a solution of $V^{(IV)}$ to $V^{(V)}$. Angular velocity $\omega = 300, 600, 900, 1200, 1500, 1800$ RPM, respectively for the curves $I = f(E)$ 1 to 6. Top/group C: Curves obtained with the cylinder alone while the disc is masked; Bottom/group D: Curves obtained with the disc alone while the cylinder is masked.

WE= rotating graphite (disc or cylinder, diameter 1 cm, height 2 cm); $[V^{(IV)}] = 1.5 \text{ mol.L}^{-1}$ in $[H_2SO_4] = 3 \text{ mol.L}^{-1}$; $S_{\text{cylinder}}/S_{\text{disc}} = (\sim \frac{63}{0.78}) \sim 8$; $r = 10 \text{ mV.s}^{-1}$; $T = 10 \text{ }^\circ\text{C}$; AE = Pt. Ohmic drop corrected with the initial value of the solution resistance (EIS).

ii: Plots of $\ln I = f(\ln \omega)$; The currents were extracted from the Fig. 3i, without subtraction of the residual current. C_1 and C_2 correspond to the cylinder at respectively 1.1 and 1.3 V; D_1 and D_2 correspond to the disc at respectively 1.1 and 1.3 V.

coefficient of the $V^{(IV)}$, these results evidence the need to determine and to compare the equations linking the mass transfer and the angular velocity for both geometries, the disc and the cylinder. It seems that the transfer is more efficient for the disc than for the cylinder, but this needs to be confirmed. The current was measured at two potentials (1.1 and 1.3 V) for both the cylinder and the disc; Then the curves $\ln I = f(\ln \omega)$ were plotted and presented in Fig. 3ii. The graph exhibits linear relations for all the examined cases:

C_1 : Cylinder at 1.1 V

$$\Leftrightarrow \ln I_{\text{at } 1.1 \text{ V, in A}} = -3.14 + 0.37 \ln \omega_{\text{rad/s}} \quad R^2 = 0.98 \quad (5)$$

C_2 : Cylinder at 1.3 V

$$\Leftrightarrow \ln I_{\text{at } 1.3 \text{ V, in A}} = -3.13 + 0.42 \ln \omega_{\text{rad/s}} \quad R^2 = 0.99 \quad (6)$$

D_1 : Disc at 1.1 V

$$\Leftrightarrow \ln I_{\text{at } 1.1 \text{ V, in A}} = -4.15 + 0.22 \ln \omega_{\text{rad/s}} \quad R^2 = 0.99 \quad (7)$$

D_2 : Disc at 1.3 V

$$\Leftrightarrow \ln I_{\text{at } 1.3 \text{ V, in A}} = -4.24 + 0.29 \ln \omega_{\text{rad/s}} \quad R^2 = 0.99 \quad (8)$$

Note that, considering the disc alone, the slope found (~ 0.2 to 0.3 as function of the potential used) is practically the half of the theoretical value predicted by the Levich law ($I_{\text{lim}} = \lambda \omega^{0.5}$) for a rotating disc electrode. This discrepancy is attributed to the fact that our operating conditions do not fulfil all criteria (indicated below) required for the application of the law:

- The ratio of "the diameter of an inert surface around the disk" to "the diameter of the electroactive surface of the disc" needs to be at the least equal to 10, to enable the correct flow of the solution. Here, because of the chosen form of the graphite cylinder, the whole surface of the disc is reactive, instead of a small disc surrounded by a Teflon non-reactive area, enabling the establishment of a stabilized and defined interfacial flow [20].
- The ratio of "the vessel diameter" to "the electrode diameter" needs to be at the least equal to 10 to avoid border effects (here the ratio is ~ 3).

Concerning the cylinder, the slope found (~ 0.35 to ~ 0.42) is also practically the half of the theoretical value predicted in the bibliography ($I_{\text{lim}} = \lambda' \omega^{0.7}$ [21]). Note that, the exponent of 0.7 was obtained with a metallic cylinder inserted between two inert

cylinders of the same diameter and a cylindrical counter electrode having a diameter larger than that of the WE. The discrepancies could be caused by: (i) a non-uniform electrical field because of the particular geometry of the chosen system: The CE is a plane plate of platinum and the current density to the rear surface area of the cylinder is very low, thus reducing its effective electroactive surface area, and,

(ii) A non-uniform flow around the bottom border of the cylinder (similarly to the disc). Here, if we assume an upward flow from the bottom of the beaker to the disc, we can conclude that the solution arriving to the disc (i.e. the basis of the cylinder) is deviated far from the cylinder, thus reducing the flux arriving to the lateral area of the electrode (possible eddies near lateral wall). However this effect seems to be cancelled as the angular speed of the electrode increases.

Another parameter which can influence the answer of the electrode could be the activation of the surface area of the graphite [18]. As a matter of fact, oxygenated groups (C-O) at the surface of the graphite seem to enhance the electrocatalytic activity of the graphite.

In the present study the electrode has been polished (as much as possible in the same conditions for all the plots), but no extra activation was performed before any recording of the current. Thus a part of its surface could remain covered by oxygenated groups while the other part is not and this is difficult to be controlled, because of the easy oxidation (chemical or electrochemical) of the graphite.

A comparison of the sum of the individual currents (surface of the disc and lateral surface of the cylinder) to the current obtained with the whole electrode (RCE) was performed and the results were presented in Fig. 4. There is practically no difference ($\Delta I < 0.6\%$ at $\omega = 300$ RPM) between both currents (2 and 4) measured at 1.1 V. For the currents measured at 1.3 V, the observed difference, even slightly higher ($\Delta I < 0.9\%$ at $\omega = 300$ RPM), remains low. Thus, the current is slightly higher for the entire WE than for the sum of the two redesigned ones; However the 'low' differences observed monotonically decrease as ω increases, and could be attributed to some disturbances, created by the adhesive scotch tape (extremities of the electrode not perfectly masked), on the solution flow. The observed effect of these disturbances mitigates as the rotation rate increases.

To sum up, the stirring affects the current but its effect is lower than the effect theoretically predicted by the correlation found in bibliography [20,21], because the operating conditions are different

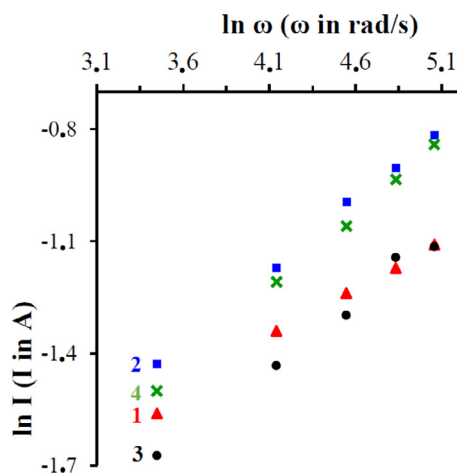


Fig. 4. Comparison of the logarithmic evolutions of the $V^{(IV)}$ oxidation currents (measured at 1.1 and 1.3 V) as a function of the logarithm of the angular velocity of the graphite WE (RCE), obtained in the two following cases:
- the whole electrode surface is operative; Curves: 1-▲ (I at 1.1V); 2-■ I at 1.3V (results extracted from Fig. 2: Graph (I)).
- the magnitude of the current corresponds to the sum of both the magnitudes of the currents obtained with the disc and the cylinder; curves: 3-● (I at 1.1 V) and 4-× (I at 1.3 V) (results extracted from Fig. 3: Graph (I)).

from those made to establish the theoretical laws used for comparison.

3.1.3. Effect of the coupled stirring rates of both the working electrode and the cross-shaped additional stirrer on the current – potential curves for the $V^{(IV)}$ oxidation

The second step is to study the effect of the cross-shaped additional stirrer on the magnitude of the current as well as on the mass transfer. To that end, several current-potential curves were plotted in various stirring conditions (not shown here to save place). Their general form is similar to the ones shown in Figs. 2 and 3.

The magnitude of the limiting current of the oxidation of the $V^{(IV)}$ to the $V^{(V)}$ was determined as a function of the angular velocity for both RCE and CSS (in the range from 300 to 1500 RPM; Both stirrers rotating in the same direction), and the results are presented in Fig. 5. The graph (I) in this figure presents the limiting current dependence on the angular velocity of the CSS, obtained for various angular velocities of the RCE. The general tendency shows that increasing the stirring causes the current to increase for both the RCE and CSS. However, a closer examination of the current evolutions shows two different areas, attributed to two behaviors:

- For angular velocities of the cross shaped stirrer $\omega_{CSS} \lesssim 600$ RPM, and for values of the $\omega_{RCE} \lesssim 900$ RPM (i.e. the first two points of the curves 1 to 3), the limiting current: (i) increases when ω_{RCE} increases, and (ii) remains practically constant when ω_{CSS} increases. For these low angular velocities, the effect of the rotation of the CSS is not perceptible because the effect of the agitation of the RCE, predominates.
- Staying at angular velocities of the CSS $\lesssim 600$ RPM, the increase of the rotation of the RCE ($1000 \lesssim \omega_{RCE}$ in RPM ≤ 1500 RPM), (i.e. the first two/three points of the curves 4 and 5) causes the limiting current of the vanadium oxidation: (i') to increase when ω_{RCE} increases, and (ii') to significantly decrease when ω_{CSS} increases.

To sum up (for the left side of the graph I), it is obvious that 'low angular speeds of the CSS' do not affect the current, while the latter decreases if ω_{CSS} increases. Assuming that the RCE causes an

Table 1

Slope values obtained from the linear regression of Eq. (4): $\ln(I) = \text{const.} + \gamma \times \ln(\omega)$ for the curves of Fig. 5– graph (II).

Cross shaped stirrer (RPM)	0	300	600	900	1200	1500
Fig. 5 graph (II), curve N°	6	7	8	9	10	11
γ $\omega_{RCE} < 600$ RPM	0.57	0.55	0.43	0.28	0.11	0.07
$\omega_{RCE} > 600$ RPM	0.57	0.55	0.47	0.44	0.42	0.40

upward flow from the bottom of the vessel to the disc, we can conclude that the rotation of the CSS prevents this motion and the solution is drifted far from the electrode, thus increasing the thickness of the diffusion layer (created by the RCE) and consequently reducing the global flux of the $V^{(IV)}$.

However, it is important here to consider this effect because when studying the suspensions, strong agitation of the CSS is necessary to supply the required power enabling the motion of the solid particles, which constitutes a goal of this study.

The right side of the curves in graph (I) of Fig. 5, corresponds to the evolution of the limiting current as a function of the angular rates of the CSS and for $\omega_{CSS} > 600$ RPM (for several rotation frequencies of the RCE). At constant rotation of the RCE, the magnitude of the current increases with the angular rate of the CSS. This is an interesting result because these 'high' angular velocities ($\omega_{CSS} > 600$ RPM) are required to allow the fluidization of the suspension. Besides, for these 'high' rotations the current also increases with the stirring of the RCE (~ 0.35 to ~ 0.6 A).

The graph (II) in Fig. 5 reports $\ln I_{lim} = f(\ln \omega_{RCE})$ for the various angular velocities of the cross shaped stirrer ($0 \leq \omega_{CSS}$ in RPM ≤ 1500). Each curve in this graph (II) reports the points obtained for one ω_{CSS} in graph (I) i.e. the points found on each perpendicular line passing through an angular velocity of the cross shaped stirrer. The curve 6, for example, presents the points (current) read on graph (I), on the vertical Y-axis, at the origin of the horizontal X-axis i.e. immobile CSS, $\omega_{CSS} = 0$.

The graph clearly shows two different shapes for the curves: The curves 6, 7 and 8, obtained at low angular rates of the stirrer (ω_{CSS} is respectively equal to 0, 300 and 600 RPM), are practically identical on the graph, and exhibit a linear evolution. This confirms the above conclusion about the 'low effect' of the agitation of the CSS on the limiting currents for $\omega_{CSS} \leq 600$ RPM. The curves 9, 10 and 11 were obtained at higher angular rates of the stirrer (ω_{CSS} equals 900, 1200 and 1500 RPM, respectively). They exhibit two different domains: on the left side the limiting current is practically constant, meaning that the stirring of the CSS cancels the effect of the stirring by the RCE and on the right side of the curves, $\ln I_{lim}$ increases linearly with $\ln \omega_{RCE}$, meaning that the mass transfer enhancement produced by the RCE predominates.

Note also that in this graph (II) the effect of the stirring of the CSS on the limiting current can be observed by the points found on each perpendicular line passing through an angular velocity of the RCE.

Table 1 provides the slopes γ of the curves $\ln I_{lim} = f(\ln \omega_{RCE})$ according to Eq. (4) (for both ranges $\omega_{RCE} < 600$ RPM and $\omega_{RCE} > 600$ RPM) obtained for a given angular velocity of the CSS. In the absence of stirring of the CSS ($\omega_{CSS} = 0$ RPM), the exponent γ is found to be equal to ~ 0.6 which is intermediate between 0.5 (disc) and 0.7 (cylinder).

For all the carried out experiments, this exponent γ decreases as the angular velocity of the CSS increases. For angular rates of the RCE lower than 600 RPM, the exponent γ is strongly affected by the rotation of the CSS, and is almost cancelled for $\omega_{CSS} = 1500$ RPM meaning that the agitation of the CSS mitigates the effect of the rotation of the RCE on the current.

Conversely, for angular rates of the RCE higher than 600 RPM, even if the coefficient γ is affected (slightly decreases from 0.47 to

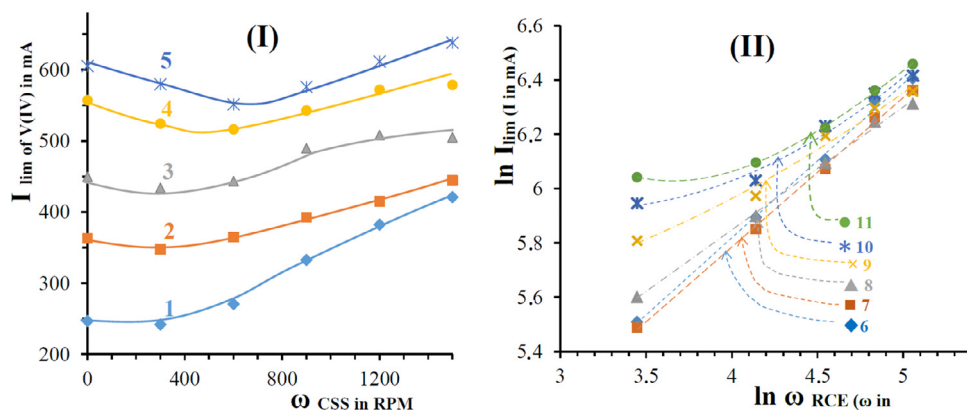


Fig. 5. Graph (I): Dependence of the limiting current of the oxidation of $V^{(IV)}$ versus the angular velocity of CSS (ω_{CSS} in RPM), for various angular velocities of the graphite RCE (each curve was obtained at constant ω_{RCE} , respectively curve N° / ω_{RCE} in RPM: 1: \blacklozenge 300; 2: \blacksquare 600; 3: \blacktriangle 900; 4: \bullet 1200; 5: \times 1500).

Graph (II): Logarithmic evolution of the limiting current as a function of the logarithm of the angular velocity of the graphite RCE ($\ln \omega_{RCE}$), for various stirring rates ω_{CSS} of the cross shaped stirrer (each curve was obtained at constant ω_{CSS} , respectively curve N° / ω_{CSS} in RPM: 6: \blacklozenge 0; 7: \blacksquare 300; 8: \blacktriangle 600; 9: \times 900; 10: \times 1200; 11: \bullet 1500). Primary data concerning the $I = f(E)$ curves: WE = rotating graphite; $[V^{(IV)}] = 1.5 \text{ mol.L}^{-1}$ in $[H_2SO_4] = 3 \text{ mol.L}^{-1}$; $r = 10 \text{ mV.s}^{-1}$; $T = 10 \text{ }^\circ\text{C}$; AE = Pt. ohmic drop corrected (EIS).

0.4), the low observed decrease translates the fact that the effect of the RCE on the flux of the vanadium transferred to the interface predominates against the effect of the CSS.

Even if the coefficient γ informs about the effect of the rotation of each element (RCE and CSS) on the transferred vanadium flux, what is important to note is that the rotation of both stirrers contributes to increase the mass transfer.

The effect of the rotation of the CSS is more significant for high (> 600 RPM) angular rates, and this:

- Is typical of the geometry of the used electrochemical cell,
- Will be very important to ensure the motion of concentrated suspensions of vanadium.

The results, obtained for a saturated solution of $V^{(IV)}$, will be used as reference in the study of the impact of solid particles on the response of the system.

3.2. Study of the solid – liquid suspensions

The presence of solid particles in the posolyte $V^{(V)} / V^{(IV)}$ (but also in the negolyte $V^{(II)} / V^{(III)}$) can significantly affect positively or negatively the performances of the battery. Indeed, as a function of the rate of the discharge or recharge of the system, precipitates can appear and as a function of their size they can stick on the electrodes and cause some passivation. Moreover, the motion of the bigger size particles close to the interface ‘electrode-suspension’ could contribute to enhance the molar flux of the active species, increasing therefore the current. In other words, the shock of the particles at the interface can be assumed to contribute to statistically reduce the thickness of the diffusion layer, thus enhancing the mass transfer. Another effect of the solids could be the decrease of the effective diffusion coefficient, and both parameters will be examined in the next section.

3.2.1. Effect of the fraction of the solid: glass spheres

Current-potential curves were plotted in suspensions made of a 0.75 mol/L solution of the $V^{(IV)}$ and various contents of inert solid glass spheres. Because their specific gravity (1.1 g/cm^3) is ‘lower than that of the vanadium acidic solution’ most of the glass spheres float, and this requires therefore a strong stirring to obtain a uniformly distributed suspension. The $I = f(E)$ curves (not shown here) have a similar shape as those obtained above; Fig. 6 shows the evolution of the current of the oxidation of $V^{(IV)}$ versus

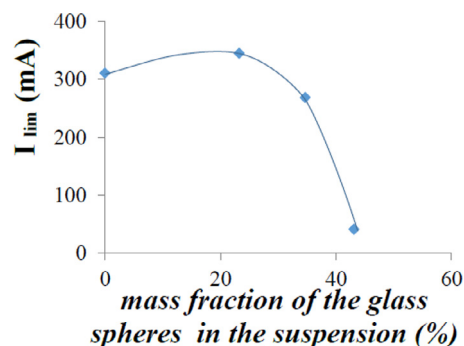


Fig. 6. Curve showing the evolution of the vanadium oxidation limiting current measured at $E = 1.1 \text{ V}$ as a function of the mass fraction of added glass spheres into a 60 mL solution of $V^{(IV)}$ at 0.75 M; $[H_2SO_4] = 3 \text{ M}$. Glass beads with a specific gravity of $\sim 1.1 \text{ g/cm}^3$ and a granulometry in the range of $9 < d_{\text{glass spheres in } \mu\text{m}} < 13$ (average diameter = $11 \mu\text{m}$).

Primary data for the monitoring of the $I = f(E)$ curves; $r = 10 \text{ mV/s}$; $T = 10 \text{ }^\circ\text{C}$; WE = graphite cylinder; RE = ECS; AE = Pt plate, CSS at 1500 RPM; RCE at 1500 RPM.

the mass percent of the spheres. The curve shows a strong influence of the solid: The measured current in the examined range varies from 0.3 A to $\sim 0.05 \text{ A}$. For low mass fraction of the spheres ($\lesssim 20 \%$) the current lightly increases ($\lesssim 15\%$), probably because an enhancement of the mass transfer of the vanadium arriving at the interface is caused by the collisions of the spheres into the diffusion layer.

However for higher fractions ($\gtrsim 30\%$) of the solid particles the current dramatically decreases until being practically cancelled for 45% of solid particles into the suspension.

The solid spheres constitute an obstacle to the dissolved vanadium motion; Their presence in the solution causes the decrease of the effective diffusion coefficient of the $V^{(IV)}$, because of the decreasing space to diffuse in the bulk.

Indeed, 50 g of the glass spheres represent a volume of solid of 45.4 mL, added into 60 mL of liquid. Assuming the additivity of the volumes is applicable (total volume of the suspension = 105.4 cm^3) and the mean diameter of the glass spheres is $d_g = 11 \mu\text{m}$ (their granulometry ranges from 9 to $13 \mu\text{m}$) then, the number of particles (6.52×10^{10} particles) represents a volumetric fraction of the solid $\phi_{\text{max}} = 0.43$ and the volume fraction available for the diffusion is $\varepsilon = (1 - \phi_{\text{max}})$.

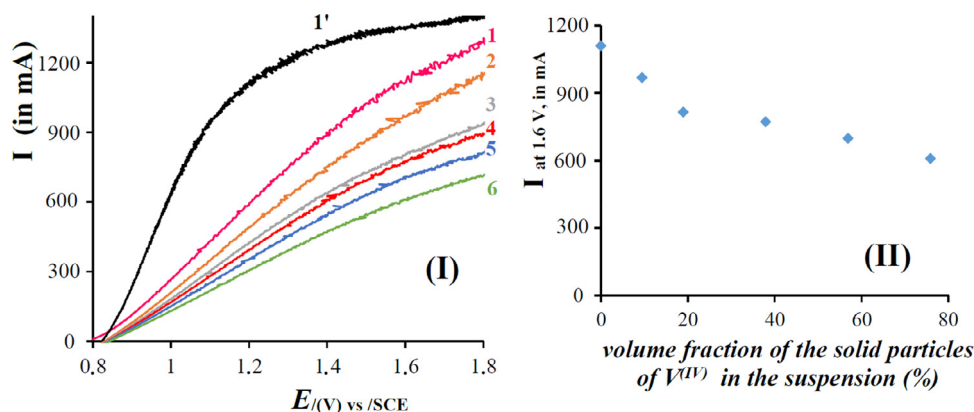


Fig. 7. Graph (I): Current potential curves obtained on a graphite RCE, immersed in Liquid-Solid suspensions containing dissolved $V^{(IV)}$ (60 cm³, at saturation i.e. 1.5 mol/L) and various mass fractions of the solid $VOSO_4 \cdot 5H_2O$ as indicated: 1/Pink: 0 g; 2/brown: 5.7 g; 3/grey: 11.4 g; 4/red: 22.8 g; 5/blue: 34.2 g; 6/green: 45.5 g (total molar quantity of the $V^{(IV)}$ in equivalent mol/L of suspension: 1.5, 1.79, 2.05, 2.5, 2.88, 3.21). Curves 1 to 6 obtained without correction of the ohmic drop. Curve 1' = the same solution than for curve 1, with corrected ohmic drop (EIS). WE = graphite RCE; CE = Pt plate; $[H_2SO_4] = 3$ M; $r = 10$ mV/s; $T = 10$ °C; $\omega_{RCE(RPM)} = \omega_{CSS(RPM)} = 1500$ RPM. **Graph (II):** Evolution of the current measured at 1.6 V as a function of the added solid particles of $VOSO_4 \cdot 5H_2O$ (For interpretation of the references to colour in this figure legend, the reader is referred to the web version of this article.).

If the glass spheres are equally dispersed into the electrochemical vessel, that represents $N_g = 641$ glass spheres per cm of distance, in a direction between the wall of the cell and the axis of the RCE.

Then, the tortuosity (9) is equal to 1.4, and enables to access the effective diffusion coefficient D_{eff} (10).

$$\tau = 1 + (\pi - 2) \times d_g \times \frac{N_g}{2} \quad (9)$$

$$D_{eff} = \frac{\varepsilon}{\tau} D = 0.41 \times D \quad (10)$$

This result shows that the diffusion coefficient falls at about 60% of its initial value, which could partially explain the current decrease, but not its complete cancellation. Note that the masking of the electrode's accessible surface by the glass spheres could also significantly affect the current.

Indeed, assuming roughly a thickness of the diffusion layer in the range from 50 to 100 μ m, it is possible to stack maximum about ten glass spheres, which represents an important barrier, even if these spheres have an important size and could relatively be easily removed from the electrode's surface.

To summarize, the enhancement in the vanadium molar flux arriving at the interface (by the motion of the spheres into the diffusion layer) is not really significant for the low fractions of the glass spheres. Furthermore, the current decreases rapidly when the fraction of added glass spheres increases, mainly because of the reduction of the available space for the diffusion of the vanadium.

3.2.2. Effects of the fraction of the $VOSO_4$ solid particles and of the stirring of the suspension

Various $I = f(E)$ curves were plotted on a graphite rotating cylinder used as anode and immersed into a suspension containing a solution saturated in $V^{(IV)}/1.5$ M and various mass fractions of solid particles of $VOSO_4$; the results are indicated in Fig. 7.

Curve 1 was obtained with the saturated solution of the dissolved $V^{(IV)}$ at 1.5 M (in $[H_2SO_4] = 3$ M). The curve exhibits a large range of overpotential (from ~0.8 to ~1.6 V) before reaching the beginning of a plateau and the corresponding limiting current. The strong shift of the $I = f(E)$ curve could be attributed (i) to a slow/partially irreversible system, but also (ii) to the significant ohmic drop because of the important current flowing ($I_{max} \sim 1.3$ A or 1.8 kA/m²). The curve 1', obtained under the same conditions, but with correction of the ohmic drop (measurement of the

resistance of the solution between the WE and the RE by EIS), exhibits a classical shape, showing (i) a limited activation overpotential range (from ~ 0.8 to ~ 1 V), and (ii) a 'diffusion-plateau' corresponding to a mass transfer limitation for the $V^{(IV)}$. This shape clearly indicates that the corresponding redox system ($V^{(IV)}/V^{(V)}$) is rapid/quasi-reversible.

The curves 2 to 6 of Fig. 7(I), obtained by adding, into the saturated solution of $V^{(IV)}$, increasing quantities of the solid $VOSO_4 \cdot 5H_2O$, show that the current (measured at 1.6 V) decreases as the amount of the added powder increases, and the decrease (until ~ 46%) reaches a pseudo-plateau for solid particles fractions higher than ~ 30% (Fig. 7, graph II).

Moreover, as the solid fraction increases the curve deformation is amplified, (for example curves 2, 3 and 6 for solid fractions respectively 10, 20 and 75%), even with an ohmic drop correction using the initial measured resistance of the solution.

Except the fact that no increase of the current was observed for the very low fractions of solid added (not examined in fact), this behaviour appears to be similar to the one observed in the case of inert glass spheres (Fig. 6), and the same conclusion can be made: The solid contributes to reduce the volume of the liquid into which the $V^{(IV)}$ diffuses, thus reducing its flux arriving to the electrode. However, because of the extended size range of the solid vanadium particles (~ 3 < d_p in μ m < ~ 600) it is not easy to carry out a rigorous and deep quantitative analysis of the system.

These results show that, at constant stirring, the increase of the fraction of the solid particles of the vanadium does not seem to significantly enhance the current. This means that, under these conditions, nor the collisions of the particles on the electrode surface, nor the dissolution of the solid particles, contribute to significantly increase the rate of the vanadium oxidation. In addition to that, for the higher fractions of the solid in the suspension (> 30%) a negative effect was observed and the current decreases, that is why it seems important to avoid operating with a liquid/solid suspension in the electrochemical reactor.

The effect of the stirring of a suspension containing a constant quantity of the $VOSO_4$ powder, on the limiting current of the vanadium oxidation, was examined and the results were indicated in Fig. 8. The curves 1a to 3a were obtained under various angular rates of the RCE keeping the CSS immobile, while for the curve 4a both the RCE and the CSS are used. The curves 1 to 3 were imported from Fig. 2 for comparison.

The curves (2a) and (3a) exhibit a classical shape with a diffusion plateau of which intensity increases with the stirring; The

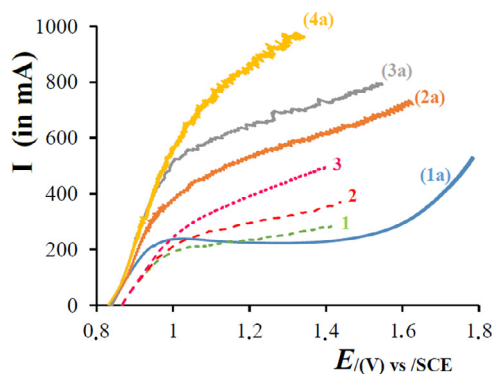


Fig. 8. $I = f(E)$ obtained for various stirring on a graphite RCE, immersed in Liquid-Solid suspension containing dissolved $V^{(IV)}$ at 1.5 mol/L and solid $VOSO_4$, the total vanadium concentration in the suspension is equivalent to 2.35 mol of $V^{(IV)}$ /litre of suspension (which corresponds to 80% of the solubility in solid form); For the curves 1a to 3a the angular velocities ω_{RCE} are 300, 600 and 1500 RPM, respectively and $\omega_{CSS} = 0$ RPM. For the curve 4a, $\omega_{RCE} = \omega_{CSS} = 1500$ RPM; Curves 1, 2 and 3 are imported from Fig. 2 for $\omega_{RCE} = 300, 600$ and 1500 RPM, respectively. WE = graphite RCE; CE = Pt plate; $[H_2SO_4] = 3$ M; $r = 10$ mV/s; $T = 10$ °C; Curves obtained with correction of the ohmic drop (EIS).

curve (1a) obtained with an angular rate of 300 RPM exhibits the same features, except that the limiting current slightly decreases for applied potentials higher than 1 V/SCE. This decrease is due to the depletion of active material in the diffusion layer; In fact, the applied stirring is insufficient to renew the interfacial layer solution, nor to lift the solid particles. This phenomenon disappears for higher stirring rates (curves 2a and 3a).

Increasing the angular rate of the RCE causes the current to increase in all the examined cases.

As a matter of fact, for the liquid-solid suspension, the logarithmic analysis of the current, measured on the curves 2a and 3a, led to the correlation (11). The same analysis performed for the curves 2 and 3 (from Fig. 2) led to the correlation (2) for which the slope is very close to the previous one: 0.27 against 0.25 (but the magnitude of the current was lower).

$$\ln I_{at\ 1.1\ V, \text{ in A}} = -1.78 + 0.25 \times \ln \omega_{\text{rad/s}} \quad (11)$$

The limiting current is enhanced when the CSS is activated (curve 4a): at 1.4 V, the current is 0.95 A, 0.7 A and 0.48 A for the curves 4a, 3a and 3, respectively. At high angular velocities ($\omega_{RCE} = \omega_{CSS} = 1500$ RPM) the coupled stirring appears to be synergistic and enhances the current.

To conclude, at a constant solid mass fraction of the suspension, the stirring appears to have a positive effect on the current, even if this effect is lower than what is theoretically expected (see previous discussion). In addition, the comparison of the magnitude of the limiting currents, (curve 2 and 2a, or 3 and 3a) shows that in presence of solid particles the current is ~ 80% higher than without particles. Under strong stirring, the vanadium mass transfer appears to be enhanced compared to the one measured in the absence of solid in the saturated solution. This behaviour is confirmed with the introduction of the additional stirring (CSS/1500RPM/curve 4a, Fig. 8). Besides, to avoid any decrease in the transferred flux of the vanadium, during a preparative electrolysis carried out under mass transfer limiting conditions (such as the condition in 1a), it is necessary to ensure sufficient stirring of the suspension.

These results are not contradictory with the results observed when studying the effect of the solid fraction on the current; Indeed, here the solid fraction remains constant and the stirring enhances the transfer, while in the previous situation the stirring remains constant and the fraction of the solid increases thus decreasing the available volume for the diffusion of the vanadium ions.

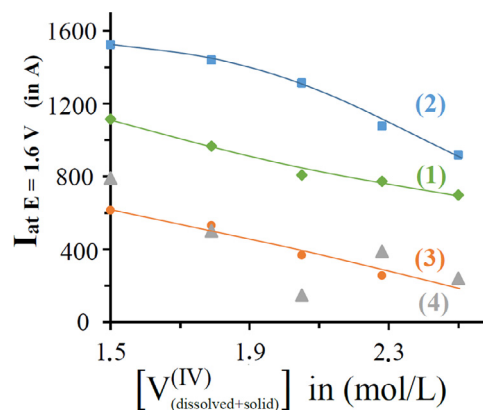


Fig. 9. Evolution of the $V^{(IV)}$ oxidation current measured at 1.6 V as a function of the added mass of the solid $VOSO_4 \cdot 5H_2O$, for various mass fractions of the ketjen black (KB). The origin of the abscises correspond to a saturated solution of the $V^{(IV)}$ (1.5 mol/L). Curves number- KB mass/ mass%: 1- 0 g/0%; 2- 0.1 g/0.12%; 3- 0.25 g/0.31%; and 4-0.7 g/0.86%. Points: Experimental results; Lines: Interpolated evolutions. Primary data for $I = f(E)$ (curves not shown here): WE = graphite RCE; CE = Pt plate; $[H_2SO_4] = 3$ M; $T = 10$ °C; $\omega_{RCE} = \omega_{CSS} = 1500$ RPM; $r = 10$ mV/s; $V_{\text{initial}} = 60$ cm³. Curves obtained without correction of the ohmic drop. The suspensions were prepared as indicated in Section 2.2.

Note that another objective of this study was to examine if the dissolution of the solid particles of the vanadium could eventually compensate its depletion in the vicinity of the interface, thus enabling an increase of the oxidation current. The obtained results do not allow to conclude on this point: indeed, because of the strong stirring (required to maintain a uniform/fluidized suspension) and the subsequent increases of the current, it is not easy to observe any effect by the dissolution of the vanadium. Moreover at constant stirring, when increasing the solid fraction, the current decreases in both cases ($VOSO_4$ or inert glass spheres); Here also it is difficult to evidence any effect of the dissolution of the vanadium particles on the current.

3.2.3. Influence of ketjen black (KB) on the oxidation current

This part aims to study, by plotting several $I = f(E)$ curves, the effect of KB on the vanadium $V^{(IV)}$ oxidation limiting current. As mentioned before, the addition of KB is expected to extend the surface of the electrode in the bulk (exploiting the adhesion of KB aggregates on the current collector) [22]. The carbon nanoparticles are suspected to induce an increase of the current by a percolation phenomenon enabling to carry out the reaction (1) or (1') in any point of the suspension. Thus the electron released by the vanadium would be driven from KB grain to KB grain up to the interface.

The following procedure was applied in order to monitor the $I = f(E)$ curves: a certain mass fraction of the KB was added into a saturated solution of $V^{(IV)}$; Then, the effect of the mass fraction of the solid particles of the $VOSO_4 \cdot 5H_2O$ was studied and the current was measured at 1.6 V. This sequence was repeated for three different mass fractions of KB.

The curve (1) in Fig. 9 obtained (without KB) for suspensions containing various mass fractions of $VOSO_4 \cdot 5H_2O$, shows that the magnitude of the current decreases when the mass fraction of the solid vanadium salt increases, a similar behaviour to that observed above (Fig. 7, §3.4.2). The introduction of a low mass fraction of the KB (0.1 g/0.12 mass%, Curve (2)) in the saturated solution ($[V^{(IV)}] = 1.5$ mol.L⁻¹, first point on the left) causes the current to increase of ~ 40% (1.52 A), thus confirming that at low fractions the KB acts as an electronic conductor enabling electronic percolation i.e. the electrons produced by the $V^{(IV)}$ oxidation can be driven by the KB aggregates from the bulk to the RCE surface in some extent length.

When $\text{VOSO}_4 \cdot 5\text{H}_2\text{O}$ solid particles are added into this suspension of V/KB (curve (2)), the current decreases and the decrease is enhanced as the mass fraction of the added vanadium solid increases. The previously involved problem of the decrease of the flux of VO^{2+} , created by the solid particles of the vanadium, could again be a possible explanation. In addition, here, the introduced solid particles of the vanadium interacts with the KB nanoparticles, thus leading to solid adducts (KB-Vanadium). These particles 'break' the KB aggregates thus preventing the electron conduction to the collector.

Note that, even if the current decreases when the% of solid vanadium increases (curve 2), its magnitude remains higher than the one measured without KB (curve 1) for all the examined fractions of the solid vanadium.

For higher fractions of KB (0.25 g/0.31% for curve 3 and 0.7 g/0.86% for curve 4), the observed current dramatically decreases when the% of solid vanadium increases. This means that a "concentrated" suspension of the KB negatively affects the vanadium oxidation current, while a "low" fraction has a beneficial effect. This strange behaviour needs many studies to be understood; A possible explanation could be that in a concentrated suspension of KB nanoparticles, in the absence of any surfactant, an agglomeration of the KB nanoparticles can occur, thus creating higher sizes aggregates which are consequently less performant against the electronic conduction in the bulk, they can even constitute more effective barriers to the $\text{V}^{(\text{IV})}$ mass transport.

To sum up, a low percentage of the KB has a noticeable beneficial effect (increase of 40%) on the $\text{V}^{(\text{IV})}$ oxidation current, but higher contents of KB become a drawback and lead to the decrease of this current.

Note that, perfect reproducibility of these results is difficult to obtain because there are various operating factors difficult to control (*polishing of the RCE, ohmic resistance of the suspension containing KB and solid $\text{VOSO}_4 \cdot 5\text{H}_2\text{O}$, perfect mixture of KB and solid $\text{VOSO}_4 \cdot 5\text{H}_2\text{O}$*). So the uncertainties of these results (Fig. 9) are estimated in the range from 10 to 15%.

4. Conclusions

The present experimental work was devoted to study the oxidation of dissolved vanadyl sulfate ($\text{VO}^{2+} \rightarrow \text{VO}_2^+$), in solution or in suspension in the presence of solid particles such as inert glass spheres, VOSO_4 particles and KB nanoparticles. Current-potential curves were plotted on a graphite rotating cylinder (RCE) in order to examine the effect of various operating conditions on the magnitude of the current. An additional cross shaped stirrer (CSS) was used for the lifting and the mobilization of the solid particles eventually present in the suspension.

The dependence of the mass transfer coefficient against the angular velocity of the RCE and of an additional cross shaped stirrer (CSS) was examined in various cases; The evolution follows a power law ($k = f(\omega^\gamma)$), with an exponent γ always lower than the theoretical value, because of the non-rigorous respect of the required operating conditions, initially set for the L ev eque correlation.

The beneficial effect observed on the mass transfer of the VO^{2+} at the interface (Fig. 6, the current increases by ~ 15%) for low (< 20%) fractions of the glass spheres, is attributed to the motion of the particles. However, increasing the solid glass spheres fraction up to 45% dramatically affects the current which falls practically to zero, because of a shrinkage of the available space for vanadium diffusion (the diffusion coefficient decreases by ~ 60%).

The effect of solid particles on VO^{2+} oxidation current was examined in order to evidence: (i) their contribution to the increase of the mass transfer at the interface and (ii) their ability to supply, by dissolution, depleted VO^{2+} in the diffusion layer. No

significant increase of the anodic current was observed for low mass fraction of the vanadium particles; Conversely, the increase of the solid fraction by ~ 30%, is detrimental to the anodic current (Fig. 7) which falls until ~ 46% (for similar reasons as for the glass spheres). Besides, as the solid fraction increases, the I-E curves are strongly deformed because of the important ohmic drop between the WE and the RE. These facts show the absence of any important beneficial effect of the dissolution of the VOSO_4 grains present into the diffusion layer at the interface electrode/solution.

On the other hand, the stirring appears to strongly affect the current (Fig. 8). Indeed, at a constant solid mass fraction in the suspension, the current increases 4 folds when the angular velocities of the RCE and the CSS increase from 300 to 1500 RPM and from 0 to 1500 RPM, respectively.

Lastly, the presence of low mass fractions of KB nanoparticles (0.12%) appears to be beneficial to the vanadium oxidation current (increase of 40%), thanks to the electronic percolation created by the KB aggregates which ensure the electrons transport to the collector. However, this benefice is attenuated when: (i) solid particles of the VOSO_4 are introduced into the suspension, and (ii) higher mass fraction of the KB nanoparticles are involved. Attractive interactions between VOSO_4 solid particles and KB nanoparticles, or even between KB nanoparticles amongst themselves (in absence of any surfactant) are probably responsible for the destruction of the KB aggregates and the disruption of the electronic conduction in the bulk.

Declaration of Competing Interest

The authors declare that they have no known competing financial interests or personal relationships that could have appeared to influence the work reported in this paper.

Acknowledgments

This study was supported by the [Agence Nationale de la Recherche](#), France. The authors would like to acknowledge L. Latapie and S. Desclaux for the technical support they provided for the accomplishment of this work.

Appendix

The limiting current (A_1) measured on a $I = f(E)$ curve is proportional to the mass transfer coefficient k .

$$I_{\text{lim}} = n F S k C_{\text{V}^{(\text{IV})}} \quad (\text{A1})$$

k can be expressed as a power law (A2) of the angular velocity ω of the stirrer using the Leveque correlation (A3):

$$k = a' + b' \times \omega^\gamma \quad (\text{A2})$$

$$Sh = a + b \times Re^\gamma \times Sc^\kappa \quad (\text{A3})$$

Indeed, substituting the Sherwood, Reynolds and Schmidt numbers (see definitions in nomenclature), the correlation becomes:

$$\frac{k d_e}{D} = a + b \times \left(\frac{v \rho d_e}{\mu} \right)^\gamma \times \left(\frac{\mu}{\rho \times D} \right)^\kappa \quad (\text{A4})$$

Assuming that the velocity v in the Reynolds number is the angular velocity of the stirring device (RCE or CSS), then the equation can be written as:

$$k = \frac{a \times D}{d_e} + (b \times D^{1-\kappa} \times d_e^{\gamma-1} \times \rho^{\gamma-\kappa} \times \mu^{\kappa-\gamma}) \times \omega^\gamma \Rightarrow k = a' + b' \times \omega^\gamma$$

This relation shows the dependence of the mass transfer coefficient to the angular velocity of the stirrer, and consequently that of the limiting current:

$$I_{\text{lim}} = n F C_V (IV) S (a' + b' \times \omega^\gamma) \Rightarrow I_{\text{lim}} = a'' \times S + b'' S \times \omega^\gamma \quad (\text{A5})$$

References

- [1] N. R. CCommittee for the National Academies Summit on America's Energy Future, The National Academies Summit on America's Energy Future: Summary of a Meeting, National Academies Press, Washington DC, 2008, doi:10.17226/12450.
- [2] C. Ponce de Leon, A. Frias-Ferrer, J. Gonzalez-Garcia, D.A. Szanto, F.C. Walsh, Redox flow cells for energy conversion, *J. Power Sour.* 160 (2006) 716–732, doi:10.1016/j.jpowsour.2006.02.095.
- [3] M. Skyllas-Kazacos, M. Rychick, R. Robins. All-vanadium Redox Battery, U.S. Patent. Application US07/145,640 events (1986); US4786567A (1988).
- [4] L.H. Thaller, Electrically rechargeable redox flow cells, in: *Proceedings of the 9th Intersociety Energy Conversion Engineering Conference, San Francisco, California, New York: American Society of Mechanical Engineers, 1974, pp. 924–928. (A75-10476 01-44) Bibliographic Code: 1974iece.conf.924T.*
- [5] L.H. Thaller, Redox flow cell development and demonstration project, *J. Power Sour.* 5 (4) (1980) 382–384, doi:10.1016/0378-7753(80)80060-7.
- [6] L. Li, S. Kim, W. Wang, M. Vijayakumar, Z. Nie, B. Chen, J. Zhang, G. Xia, J. Hu, G. Graff, J. Liu, Z. Yang, A stable vanadium redox flow battery with high energy density for large scale energy storage, *Adv. Energy Mater.* 1 (2011) 394–400, doi:10.1002/aenm.20110000.
- [7] F. Rahman, M. Skyllas-Kazacos, Vanadium redox battery: positive half-cell electrolyte studies, *J. Power Sources* 189 (2) (2009) 1212–1219, doi:10.1016/j.jpowsour.2008.12.113.
- [8] K. Kitoh, H. Nemoto, 100Wh Large size Li-ion batteries and safety tests, *J. Power Sources* 81-82 (1999) 887–890, doi:10.1016/S0378-7753(99)00125-1.
- [9] L.Cao M.Skyllas-Kazacos, M. Kazacos, N. Kausar, A. Mousa, Vanadium electrolyte studies for the vanadium redox battery, a review, *ChemSusChem* 9 (13) (2016) 1521–1543, doi:10.1002/cssc.201600102.
- [10] C. Chanyong, K. Soohyun, K. Riyul, C. Yunsuk, K. Soowhan, J. Hoyoung, H. Yang, K.H.T. Jung, A review of vanadium electrolytes for vanadium redox flow batteries, *Renew. Sustain. Energy Rev.* 69 (2017) 263–274, doi:10.1016/j.rser.2016.11.188.
- [11] S. Kim, E. Thomsen, G. Xia, Z. Nie, J. Bao, K. Recknagle, W. Wang, V. Viswanathan, Q. Luo, X. Wei, A. Crawford, G. Coffey, G. Maupin, V. Sprenkle, 1kW/1kWh advanced vanadium redox flow battery utilizing mixed acid electrolytes, *J. Power Sour.* 237 (2013) 300–309, doi:10.1016/j.jpowsour.2013.02.045.
- [12] S. Peng, N.F. Wang, X.J. Wu, S.Q. Liu, D. Fang, Y.N. Liu, K.L. Huang, Vanadium species in CH₃SO₃H and H₂SO₄ mixed acid as the supporting electrolyte for vanadium redox flow battery, *Int. J. Electrochem. Sci.* 7 (2012) 643–649.
- [13] M. Skyllas Kazacos, M. Kazacos, Stabilized vanadium electrolyte solutions for all-vanadium redox cells and batteries, Patent US6562514B1, 2003.
- [14] R. El-Hage, F. Chauvet, B. Biscans, L. Cassayre, L. Maurice, T. Tzedakis, Kinetic study of the dissolution of vanadyl sulfate and vanadium pentoxide in sulfuric acid aqueous solution, *Chem. Eng. Sci.* 199 (2019) 123–136, doi:10.1016/j.ces.2019.01.024.
- [15] M. Vijayakumar, Liyu Li, Gordon Graff, Jun Liu, Huamin Zhang, Zhenguo Yang, Jian Zhi Hu, Towards understanding the poor thermal stability of V⁵⁺ electrolyte solution in vanadium redox flow batteries, *J. Power Sour.* 196 (7) (2011) 3669–3672, doi:10.1016/j.jpowsour.2010.11.126.
- [16] K. Post, R.G. Robins, Thermodynamic diagrams for the vanadium water system at 298K, *Electrochim. Acta* 21 (1976) 401–405.
- [17] W. Wang, Z. Wei, W. Su, X. Fan, J. Liu, C. Yan, C. Zeng, Kinetic investigation of vanadium (V)/(IV) redox couple on electrochemically oxidized graphite electrodes, *Electrochim. Acta* 205 (2016) 102–112, doi:10.1016/j.electacta.2016.04.109.
- [18] A. Hassan, T. Tzedakis, Enhancement of the electrochemical activity of a commercial graphite felt for vanadium redox flow battery (VRFB), by chemical treatment with acidic solution of K₂Cr₂O₇, *J. Energy Storage* 26 (2019), doi:10.1016/j.est.2019.100967.
- [19] M. Eisenberg, C.W. Tobias, C.R. Wilke, Ionic mass transfer and concentration polarization at rotating electrodes, *J. Electrochem. Soc.* 101 (6) (1954) 306–319.
- [20] B. Trémillon, *Electrochimie Analytique Et Réactions En solution*, Dunod, 1993 Tome 1- ISBN : 978-2-225-84177-4; Tome 2- ISBN : 978-2-225-84255-9.
- [21] D.R. Gabe, F.C. Walsh, The rotating cylinder electrode: a review of development, *J. Appl. Electrochem.* 13 (1983) 3–21, doi:10.1007/BF00615883.
- [22] L. Madec, M. Yousry, M. Cerbelaud, P. Soudan, D. Guyomard, B. Lestriez, Electronic-vs-ionic limitations to electrochemical performance in Li₄Ti₅O₁₂ based organic suspensions for lithium redox flow batteries, *J. Electrochem. Soc.* 161 (5) (2014) A693–A699, doi:10.1149/2.035405jes.